APPLICATION OF H_∞ CONTROL TO A VARIABLE RESONANCE STABILISATION MECHANISM

David Anderson*, Nick Brignall†
*Industrial Systems & Control Ltd., University of Strathclyde, Glasgow, UK
†BAE SYSTEMS, Sensor Systems Division, Edinburgh, UK

Keywords: Servomechanism, variable resonance, H-Infinity, stabilisation, uncertainty

Abstract

This paper describes the application of H_∞ design synthesis to the control of a mechanical stabilisation system with uncertain and time-varying first structural resonance frequency. The class of mechanisms under investigation is described and the design aims and classical control techniques currently employed are presented. It is shown that both an increase in performance and robustness to mechanism uncertainty can be achieved.

1 Introduction

Platform stabilised systems are becoming increasingly prevalent on both new-build and refit military land, sea, air and space programmes. Systems such as airborne electro-optic pointing & tracking, navigation, satellite positioning, shipboard weapon aiming and tank gunnery sights all rely on a platform stabilisation mechanism of some kind. Of these systems, often the highest performance specifications are applied to electro-optic (EO) systems. Although research is ongoing for new methods of stabilisation (such as phased-array beamsteering & digital image stabilisation), current EO systems precision line-of-sight (LOS) stabilisation is often realised through a stabilised mirror mechanism.

A stabilised mirror is often *the* critical stabilisation mechanism in an electro-optic system. Essentially, it is a small, two-axis gimbal mechanism with the mirror mounted on the inner gimbal. Connected to the mirror via a 2:1 reduction drive is a separate shaft housing two gyroscopes whose measurement axes are aligned with the LOS. As the gyroscope maintains orientation with respect to an inertial reference, the LOS angular position with respect to inertial space can be measured. Actually, the gyros pick-off coils measure the deviation of the gimbal axes from the inertial (spin) axes, which is the error signal in a feedback loop to the motors on each gimbal. The motors then torque the gimbal set to maintain the LOS along an inertial vector, thus stabilising against the motion of the host platform.

In most stabilised EO systems, overall performance is critically dependant on the accuracy of the stabilisation sub-system. More stringent operational requirements, such as increased stand-off ranges, will typically necessitate higher resolution focal plane array cameras and narrow field-of-view optics. This in turn imposes a smaller jitter budget on the sightline stabilisation system, which can only be achieved through iterative optimisation of the mechanical, optical, sensor and actuator design. Central to this process however, is the design of the control law.

The critical performance parameter for a platform stabilisation system is the compliance, or stiffness, of the controller [4], [8], i.e., how much the LOS changes to a unit disturbance torque. There are four main sources of disturbance torque – bearing friction, motor drag (through back-EMF coupling), mass imbalance and mirror accelerating torques [9]. Of these, the most critical to compliance is the bearing friction. Friction effects can be reduced either through adaptive friction compensation schemes (not be considered here) or by increasing the bandwidth of the controller. However, the controller bandwidth is limited by i) phase lag induced by finite sensor bandwidth ii) limitations imposed by sampling rate/latency in the case of digital control and iii) the frequency of the first structural/mechanical resonance. Resonance limitations can be mitigated by using tuned notch filters (pole-zero cancellation) assuming that the frequency of the resonance is known and constant.

The system under consideration in this investigation will not be named for obvious reasons but (in common with many stabilised mirror mechanisms), exhibits a resonance associated with the mechanical linkage between the mirror and gyro platform. A schematic of the mirror assembly is shown in figure 1.

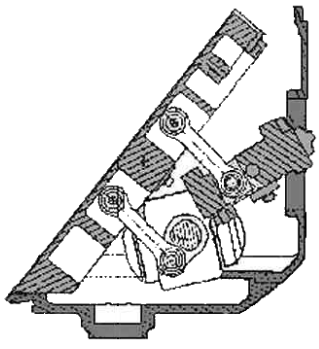

Figure 1: Schematic of the stabilised mirror mechanism

In meeting the volume and packaging constraints, the mechanical design of the mirror mechanism is such that the orientation of the system influences the frequency of the resonance, which also varies substantially between mechanisms. As a consequence, each mechanism's compensation has to be individually tuned which means a

store of all possible notch filter kits (currently 5) must be kept, (which along with the time required to individually tune each mechanism, impacts profitability). As the resonance is orientation-dependant, care must be taken that the controller cannot de-tune during operation.

The servo compensation on this type of mirror is limited by the resonance of the mechanical linkages between the gyro platform, mirror and balancer [7]. The existing compensator is a phase-lead type, augmented with a state-space pole-zero cancellation filter, de-tuned to provide attenuation in the presence of resonance drift. The resonance nominally has a frequency of around 200Hz, which coincidentally is the frequency of the gyro swash. To combat this noise source, a 200Hz notch filter is placed on the gyro output which also helps to control the influence of the resonance in the closed loop. The gyro signal also passes through three other notch filters, each specifically tuned to attenuate a gyro noise source. This servo arrangement performs well enough, although the resonance drift has forced the servo bandwidth and closed loop stiffness below the original desired values.

The aim of this investigation was therefore to design a controller that is robust to variations in the frequency of the resonance while simultaneously improving the compliance. As both of these objectives can be combined into a single H_∞ norm minimisation problem (robust performance), H_∞ synthesis is a natural framework for designing a viable controller. Applying H_∞ controllers to flexible stabilised platforms is nothing new (see [6], [2] & [3]), however controlling over such a wide range of resonance frequencies is. The interesting result of this study was the quality of the controller obtained against the specific nature of the problem.

2 Mathematical Model

The stabilised mirror mechanism shown in figure 1 can be adequately approximated by a three-mass, lumped parameter model with a flexible connection between each mass, figure 2.

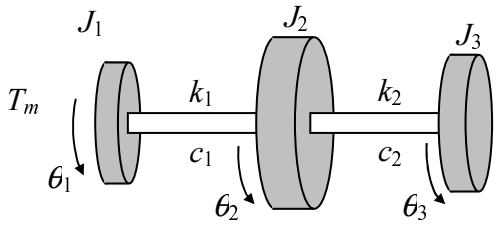

Figure 2: Free-body diagram of the mirror mechanism

From this diagram, the equations of motion for the mechanism alone can be shown to be,

$$\begin{aligned} J_1\ddot{\theta}_1 &= T_m + c_1(\dot{\theta}_2 - \dot{\theta}_1) + k_1(\theta_2 - \theta_1) \\ J_2\ddot{\theta}_2 &= c_1(\dot{\theta}_1 - \dot{\theta}_2) + k_1(\theta_1 - \theta_2) + c_2(\dot{\theta}_3 - \dot{\theta}_2) + k_2(\theta_3 - \theta_2) \\ J_3\ddot{\theta}_3 &= c_2(\dot{\theta}_2 - \dot{\theta}_3) + k_2(\theta_2 - \theta_3) \end{aligned} \quad (1)$$

The values of k_1, k_2, c_1 and c_2 were obtained by curve fitting in the frequency domain to match the estimated transfer functions obtained by experiment from the actual mechanism. Although the mirror assembly dynamics are much more complex than this simple model can depict, the dominant transfer function characteristics were captured. Indeed, this model was sufficiently representative for use in the design of the original compensator. It should be noted that this model was validated by experiment against several mechanisms to be a good representation of the dominant mechanism response.

The second stage of the modelling exercise concerns the simulation of the brushless DC motor. A standard DC motor model was used [5] assuming constant, known torque coefficient, back-EMF coefficient, armature resistance and inductance. The motor is voltage driven with base-motion disturbance coupling through the back-EMF minimised by integral action in the compensator.

Finally, a gearing of 2:1 is included in the linkages to remove the effect of optical doubling and refer the sightline position to an inertial axis set.

3 Controller Design

Recall that there are two specifications on the control i) that the closed-loop stiffness is improved and ii) that robust performance is maintained over the spread of possible resonance frequencies . Consider the block diagram of figure 3.

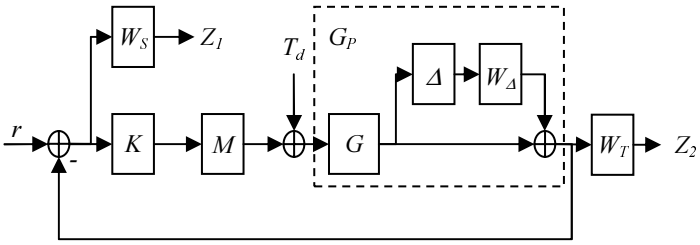

Figure 3: Stabilised mirror block diagram

Figure 3 is the mirror equations of motion represented in standard form [12] with G the nominal mechanism transfer function, M the motor transfer function, K the compensator, W_S & W_T shaping filters and Δ representing mechanism uncertainty. The transfer function from torque disturbance to output (compliance) is SG where the sensitivity $S=(I+L)^{-1}$ and $L=GMK$ is the loop gain. It is obvious that to minimise the effect of a torque disturbance (friction) on the output, the sensitivity function should be small. Alternatively, finding a stabilising controller K such that

$$\left\| W_S(j\omega)S(j\omega) \right\|_\infty < 1 \quad (2)$$

will shape the compliance through the dynamic weighting $W_S(j\omega)$ applied to the error signal. The uncertainty in the frequency (and damping) of the first resonance of the

mechanism structure can be represented by a complex, multiplicative uncertainty on the output such that;

$$G_P = (1 + W_\Delta \Delta)\, G_0\,, \quad \Delta \in RH_\infty \quad , \quad \|\Delta\|_\infty \le 1 \qquad (3)$$

The weighting (W_Δ) was obtained simply by perturbing the plant between the (known) upper and lower bounds of the uncertainty. For the mirror, this involved moving the frequency of the resonance between the limits described in Table 1 above. The multiplicative uncertainty associated with the perturbed plant is given by,

$$W_\Delta \Delta = \frac{G_P - G_0}{G_0} \qquad (4)$$

A plot of the multiplicative uncertainty is shown in figure 4, for ±18% deviation of the resonance frequency (maximum range over all mechanisms). This range encompasses the total deviation over all four mechanisms. This graph clearly shows the regions where the perturbed plant differs from the nominal. At low and high frequencies (with respect to the resonance frequency) the magnitude of the uncertainty is very small as the plant is well known in these regions. In the vicinity of the resonance frequencies, the uncertainty is large, as expected.

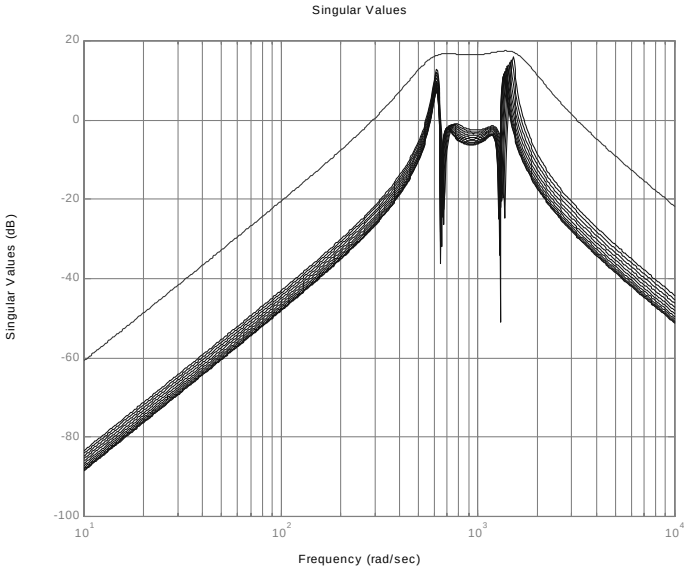

Figure 4: Multiplicative uncertainty and bounding function.

3.1 Design for Robust Performance.

A control system is said to be robust if it maintains stability and performance in the presence of differences between the actual system and the model of the system used to design the controller. Nominal performance is guaranteed if $\|W_S S_0\|_\infty \le 1$ (or $|W_S S| < 1 \;\; \forall \omega$). Robust performance requires that the nominal performance condition holds for all possible plants, including the worst-case uncertainty [11].

$$RP \;\Leftrightarrow\; |W_S S_P| < 1 \qquad \forall S_P, \forall \omega \qquad (5)$$

It can be shown, by considering Nyquist criterion that robust performance for a SISO system is given by,

$$RP \;\Leftrightarrow\; \max_\omega \left(|W_S S| + |W_\Delta T| \right) < 1 \qquad (6)$$

This condition can be very closely approximated by the standard mixed-sensitivity H_∞ condition,

$$\left\| \begin{matrix} W_S S_o \\ W_\Delta T_o \end{matrix} \right\|_\infty = \max_\omega \sqrt{|W_S S_o|^2 + |W_\Delta T_o|^2} < 1 \qquad (7)$$

to within a factor of at most $\sqrt{2}$, i.e., if the performance bounds on the sensitivity function and the robust stability bounds on the complementary sensitivity function are met, the loop will exhibit robust performance.

An unfortunate side issue of the mixed-sensitivity H_∞ approach is that the plant should ideally not have any $j\omega$-axis poles or zeros [1],[10]. The simple cure is to replace s with (s+ε) for some small number ε. However, this changes the relative position of the poles and zeros of the plant, so the more accurate solution is to use a bilinear transform to move the whole plant into the LHP, design the controller, then move the controller back by the exact same amount. The inconvenience is offset however, because the transformation adds an additional design parameter as the sensitivity function changes with how far the plant model has been shifted. The bilinear transform is given by,

$$s = \frac{\tilde{s} + p_1}{\frac{\tilde{s}}{p_2} + 1} \qquad (8)$$

where the numbers $-p_1$ and $-p_2$ are the end-points of the diameter of a circle in the left *s*-plane that is mapped by the equation above onto the $j\tilde{\omega}$ -axis in the $\tilde{s}$ -plane. The bilinear transformation preserves the performance, but in practice p_1 and p_2 must be appropriate to the problem.

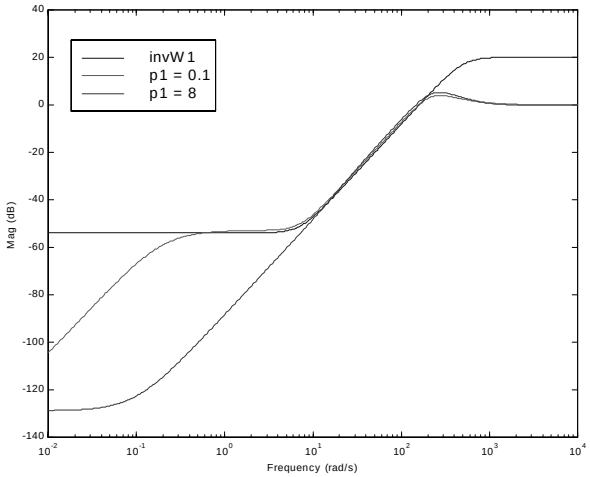

Figure 5: The effect of bilinear shifting on the shape of the sensitivity.

As an example consider figure 5. This diagram illustrates the shape of the sensitivity function corresponding to two shifts of p_1 = -0.1 and p_1 = -8. For the lower value of p_1, the sensitivity remains closer to the inverse weighting function in the vicinity of the low frequency breakpoint than for p_1 = -8. As the design aim is to minimise the sensitivity function at low frequencies, the faster roll-on and, by extrapolation, the better design, is obtained by using p_1 = -8. Selection of p_1 is an iterative procedure, terminated when the design specifications are met.

Other methods do exist for overcoming the limitations of the mixed-sensitivity approach when controlling a plant with $j\omega$-axis poles or zeros, most notably the technique of introducing integral action into the sensitivity weighting.

4 Results

The sensitivity weighting function was specified as follows,

$$W_S(s) = \frac{\beta(\alpha s^2 + 2\zeta_1\omega_c\sqrt{\alpha}s + \omega_c^2)}{(\beta s^2 + 2\zeta_2\omega_c\sqrt{\beta}s + \omega_c^2)} \qquad (9)$$

after several iterations, the parameters of this weight selected for this example design were, β = 500; α = 0.5; ω_c = 160; ζ_1 = ζ_2 = 0.7. ω_c was set at 160rad/s to force an increase of bandwidth but also has the added effect of acting as a tuning parameter for improving the stiffness as it increases the DC gain of the controller.

The complementary sensitivity weighting function was composed of two terms, one for specifying the closed-loop high-frequency response and the other to allow for model uncertainty. The nominal part of the complementary sensitivity weighting is,

$$W_T = \frac{s^2}{\omega_{BT}^2} \qquad (10)$$

where ω_{BT} = 600 rad/s. The second part of this weighting function must be a transfer function satisfying the upper bound magnitude limits of the multiplicative uncertainty plot, i.e. the gain must be higher than all the lines in figure 4. Several estimates of this transfer function were tried. The first transfer function examined was an almost exact fit of the upper bound, generated by combining two highly-underdamped second order poles with an s^2 term in the numerator. This transfer function yielded controllers which were only marginally stable. The second transfer function was a much simpler fit, figure 4,

$$W_{BM} = \frac{8e6s^2}{s^4 + 1197s^3 + 1.166e9s^2 + 8.649e11} \qquad (11)$$

This weighting resulted in a stable controller. Simplifying the bound still further by removing the roll-off resulted in an overly conservative specification which required the bandwidth of the sensitivity weighting lowered for the algorithm to find a stabilising controller. The final complementary sensitivity weight was selected as,

$$W_T = \frac{s^2(s^4 + 1197s^3 + 1.166e9s^2 + 8.649e11 + \omega_{BT}^2 8e6)}{\omega_{BT}^2(s^4 + 1197s^3 + 1.166e9s^2 + 8.649e11)} \qquad (12)$$

With these weightings, a 13th order H_∞ controller was computed (figure 6).

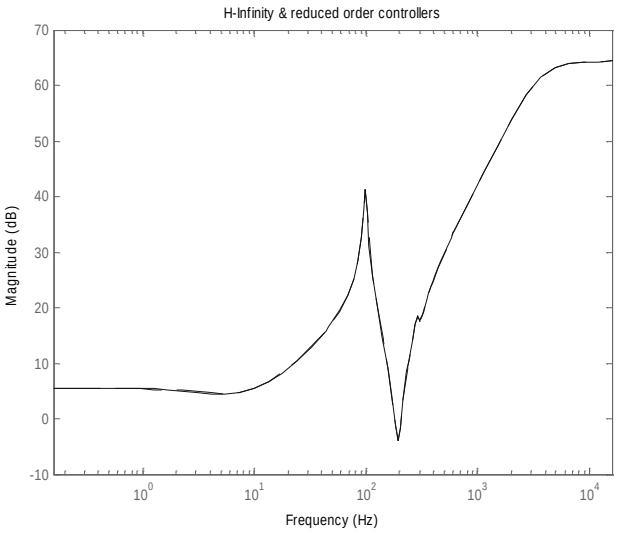

Figure 6: magnitude plot of full & reduced-order controllers/

The unfortunate feature of the controller is the rise in gain at frequencies beyond 700 Hz, which results in much of the high frequency gain lift of 60 dB. This figure is far beyond that of the baseline controller, which peaks at about 35 dB. It is not clear whether any real use is made of this gain rise, or whether it is simply a consequence of the weights used in the design. However, the H_∞ algorithm fails to produce a stable controller if specific efforts are made to reduce this gain through normal sculpting of either the control or complementary sensitivity weightings.

Schur BST-REM balanced residualisation and the optimal Hankel norm model reduction algorithms were applied to reduce the controller order. The Hankel norm algorithm performed very poorly in comparison to the Schur BST-REM algorithm. After a process of trial and error, a 9th order model was settled upon. The 4 states removed from the controller had a negligible impact on the controller input-output structure as no real degradation in performance was observed (figure 6). Reducing the order still further yielded stable controllers, but the phase margins were significantly reduced. The lower limit for this operation was about 6th order.

Controller performance was assessed against the robustness to changes in the resonance frequency. To fully exercise the controller, the perturbed plant has the resonance peak located at the farthest spread distance over the four mechanisms. The step response the H_∞ servo is shown in figure 7. The H_∞ controller performs well with a minor resonance-induced oscillation impacting on the response. It is worth noting at this point that the classically-designed controller would have experienced significant difficulty under this test condition.

Compliance plots for the existing, baseline controller and the H_∞ controller are shown for comparison in figure 8. It is obvious that the new controller is stiffer than the baseline, yielding improved rejection of friction torque. Taking the DC levels, the gain is almost half (0.06 compared to 0.112), increasing the loop stiffness by a factor of 1.867. Comparing the peaks, this reduces to 1.42, still over a 40% improvement.

The concerns regarding the high frequency gain of the controller were shown to be founded by inspection of the noise transfer function (the transfer function from the gyro signal to the motor input when the feedback loop has been closed). It is obvious from figure 9 that the control signal will be highly sensitive to sensor noise (1mV at the gyro gives 10V at the motor over the band 2-10 KHz). High loop gain roll-off minimises the impact of sensor noise on the output. However, because the control signal is subject to a voltage limit, excessive noise reduces the effective range over which accurate control can be achieved. If the noise on the sensors is significant (cheap/old sensor technology) the NTF would prohibit deployment of the H_∞ controller. Low noise sensor technologies (such as fibre-optic gyros) should alleviate this problem however.

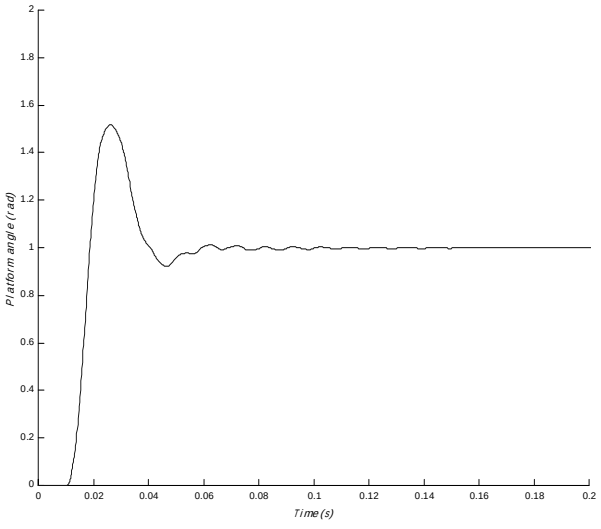

Figure 7: Step response of the perturbed servo (0.01s step on time).

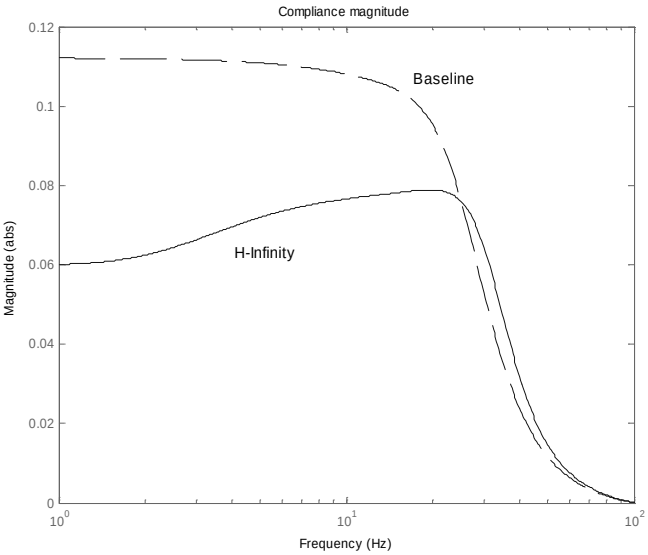

Figure 8: Compliance of existing & H_∞ controllers.

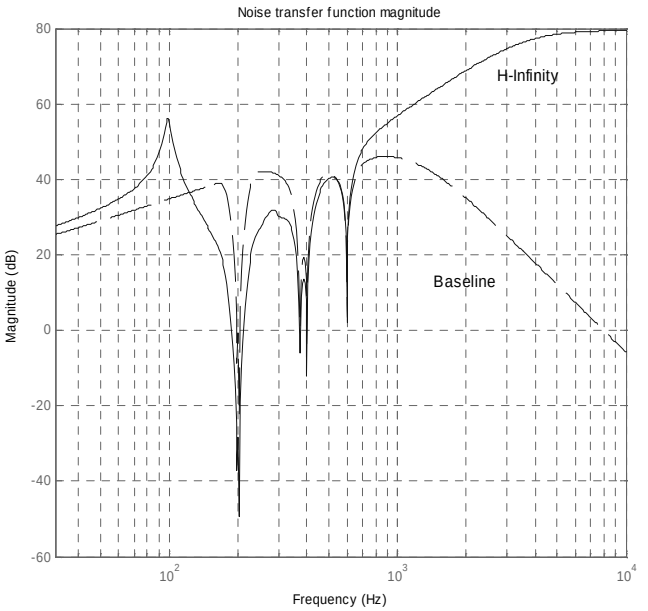

Figure 9: Noise transfer functions of existing & H_∞ controlled servos.

Converting the controller to digital form would raise a number of issues. The first is that the digitisation rate required for the fastest pole is quite at high at over 10 kHz, and the computation load would be significant, given the complexity of the controller. Any of the standard means of conversion could be used, although the bilinear method would probably be used for the first attempt. The main problem is that the robustness of the system can no longer be guaranteed - the sampler adds phase shift to the plant which was not allowed for in the design. However, the effect should be confined to higher frequencies.

5 Conclusions

The particular application presented a good design benchmark because the conventional controller is not robust across an adequate range of plant resonances, and it thus provided an opportunity for investigation of this claim of H_∞ design.

The Bilinear transform was shown to provide a useful additional design degree of freedom, without which it is doubtful an acceptable controller would have been found.

The objective of achieving a robust controller of adequate performance was met, indicating that H_∞ design methods are applicable to certain classes of servo-mechanism. However, the design achieved had excessive noise bandwidth, so further development would be required for a practical controller.

References

[1] Chiang, R.Y. and Safonov, M.G., "*Robust Control Toolbox*", User's Guide. The MathWorks Inc., Natick, MA, 1992.

[2] Coustal, P., Coville, A., Michelin, J-M., "*A Discrete Control for a Two-Axis Sight System with Structural Flexibilities*," European Control Conference, Grenoble, France, July 1991.

[3] Coustal, P., Michelin, J-M., "*Industrial Application of an H-infinity Design Method for Flexible Structures*", IEEE Control Systems, Vol. 14, no. 4, pp 49-54, August 1994.

[4] Gerson, G., Rue, A.K., "*Chapter 22 – Tracking Systems*", The Infrared Handbook, Department of the Navy, 1978.

[5] Hendershot, J.R., Miller, T.J.E., "*Design of Brushless Permanent-Magnet Motors (Monographs in Electrical and Electronic Engineering, 37)*", Motorsoft, 1994.

[6] Michelin, J-M., Coustal, P., "*Control of a Sight System Flexible Structure, A H_∞ Design,*" Proc. 30th Conference on Decision and Control, Brighton, England, December 1991.

[7] Netzer, Y., "*Line-Of-Sight Steering and Stabilization,*" Optical Engineering, Vol. 21, January-February 1982.

[8] Rue, A.K. "*Stabilization of Precision Electro-Optical Pointing and Tracking Systems*," IEEE Trans. Aerospace Electron. Sys., AES-5, No. 5, September 1969.

[9] Rue, A.K. "*Precision Stabilization Systems,*" IEEE Trans. Aerospace Electron. Sys., AES-10, No. 1, January, 1974.

[10] Safonov, M.G., "*Imaginary-Axis Zeros in Multivariable H_∞ Optimal Control*", in Modelling, Robustness and Sensitivity Reduction in Control Systems, Springer-Verlag, New York, 1987.

[11] Skogestad, S., and Postlethwaite, I., "*Multivariable Feedback Control*", John Wiley & Sons, 1998.

[12] Zhou, K., Doyle, J.C., Glover, K. "*Robust and Multivariable Control*", Prentice Hall, 1996.